Indian Journal of Pure & Applied Physics
Vol. 60, November 2022, pp. 933-940
DOI: 10.56042/ijpap.v60i11.63830

Calculation of the Surface Charge Concentration on the Argon's Dielectric Barrier Discharge: Effect of the Amplitude Voltage

Abdelaziz Bouchikhi[a]* & Abdelkhalek Bouchikhi[b]

[a]University of Saïda, Faculty of Technology, Department of Electrical Engineering, 20000 Saïda, Algeria
[b]Rue Dominique Clos, 31300 Toulouse, France

Received 16 June 2022; accepted 18 October 2022

In this work, we study the argon dielectric barrier discharge with metastable atom density on capacitively coupled radio frequency at a pressure of 1 Torr. The parameter transports of argon are depending on the electron energy and their range is about of 0.04-42 eV. A one-dimensional fluid model and the drift-diffusion theory are used to describe the argon dielectric barrier discharge. The effect of the amplitude voltage on the properties of argon dielectric barrier discharge is presented on the cycle-averaged regime. Especially the electron temperature, electric potential and metastable atom density illustrate our results on figures of merits. Consequently, these quantities increase with the increasing of the amplitude voltage. Besides surface charge concentration and the gap voltage increase too.

Keywords: Physics of Gases; Plasmas; Electric Discharges

1 Introduction

Glow discharge plasma[1-13] produced by a powered DC or RF source has extendedly various applications in industrial technologies and medical therapy. Among which, an improved discharge by substance vapour deposition, a surface adaptation by different material and plasma etching. Furthermore, a capacitive geometry can enhance these technologies[14]. The latter is a progression technique to control the discharge by means of dielectric barrier[15-18] at a low or a higher-pressure-gas. In the medical domain, we find the dermatology treatment by means of coherent and incoherent ultraviolet (UV) and vacuum ultraviolet (VUV) radiation from glow source.

Beside the experimental tools[19], the mathematical model is the best approach to describe and to optimize the discharge behaviour mostly at the electrodes sides and in the bulk plasma. Samir *et al.*[20] have investigated the effect of gas pressure on the capacitively coupled radio-frequency (CCRF) argon gas discharge. Thus, the electric potential increases and the electron temperature decreases with increasing gas pressure. Liu *et al.*[21] have studied the effect of secondary electron emission coefficient (SEEC) on the capacitively coupled RF (CCRF) argon glow discharge. They have demonstrated that increasing SEEC changes consequently many parameters such as net power absorption, electron power dissipation and thermal conductive term. Becker *et al.*[22] have presented a comparative study between argon and helium CCRF discharge by means of advanced fluid model and particle-in-cell/ Monte Carlo code.

Barjasteh & Eslami[23] have described the behaviour discharge in DBDs at a low-pressure for gas mixture (90%Ar–10%Cl_2). They have shown that the electronegativity properties and the radiation process grow when the voltage amplitude increases. However, when the frequency increases, the electronegativity properties decreases. Barjasteh *et al.*[24] have studied the effect of the voltage parameters on the characteristics of the dielectric barrier discharge (DBDs) at a low-pressure argon gas. It has been shown that an increase in applied voltage and voltage frequency lead to grow both the radiation process within the plasma and the discharge current.

In this work, we have interested to give a detail description for the behaviour of argon glow discharge operated in CCRF and controlled by dielectric barrier in presence of a metastable atom density. Moreover, we have investigated the amplitude voltage effect on the plasma characteristics.

2 Physical model and boundary condition

A description of the adopted discharge scheme is depicted in Fig. 1. As we assume that the electrode

*Corresponding authors: (Email: bouchikhiabdelaziz1@yahoo.fr)

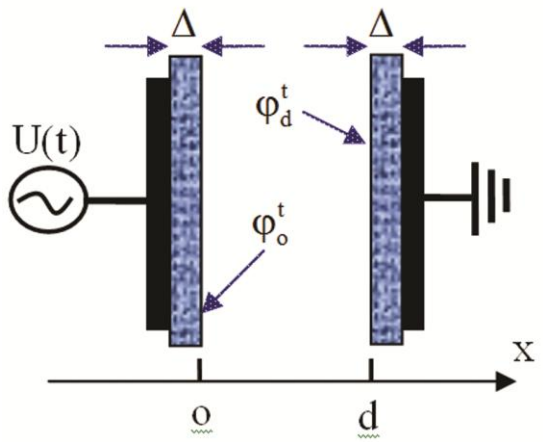

Fig. 1 — Discharge configuration, φ_x^t is the electric potential at the dielectric side.

side is greater than the inter-electrodes spacing the model has been computed in a one-dimensional geometry. Then, the fluid model is utilized to modelling the RF argon plasma. Where the frequency of the RF power supply is set to 13,56 MHz, and the argon gas pressure is equal to 1 Torr. Therefore, the RF driving frequency is less than the momentum transfer collision frequency.

In order to get a complete explanation of the low-pressure argon plasmas, both argon atoms and ions as well as excited atomic ions have been taken in account. The kinetic scheme of processes takes into account five electron collision reactions: elastic collisions, ionization, excitation, de-excitation and stepwise ionisation related to rate coefficients depending on the mean electron. These reactions are labelled as follows: P_{ec}, k_{io}, k_{ex}, K_{dex} and K_{io}^{m}, respectively. In addition, chemo-ionisation (K_{ci})[25] and radiation processes (τ_m) [26] are considered. Table 1 summarizes these reactions and their references. The processes k_{io}, k_{ex} and K_{dex} are calculated using BOLSIG+ software[27-28], and the process K_{io}^{m} is determined according to the expression given by Vriens & Smeets[29].

Then, the model[8-9] is described as follows:

$$\frac{\partial n_e}{\partial t}+\frac{\partial \Gamma_e}{\partial x}=S_e, \quad \ldots (1)$$

$$\frac{\partial n_+}{\partial t}+\frac{\partial \Gamma_+}{\partial x}=S_+, \quad \ldots (2)$$

Table 1 — Kinetic scheme of processes and their rate coefficients ((eVs^{-1}), (cm^{3}s^{-1}), (s) and (cm^{6}s^{-1}))

N°	Processes	Rates coefficients	Refs.
P_1	$Ar + e^- \rightarrow Ar + e^-$	P_{ec}	30
P_2	$Ar + e^- \rightarrow Ar^+ + 2e^-$	k_{io}	27-28
P_3	$Ar + e^- \rightarrow Ar_m^* + e^-$	k_{ex}	27-28
P_4	$Ar_m^* + e^- \rightarrow Ar + e^-$	K_{dex}	27-28
P_5	$Ar_m^* + Ar_m^* \rightarrow Ar^+ + e^- + Ar$	$K_{ci} = 8.1\times10^{-10}$	25
P_6	$Ar_m^* \rightarrow Ar + h\nu$	$\tau_m = 10^{-7}$	26
P_7	$e^- + Ar_m^* \rightarrow Ar^+ + 2e^-$	K_{io}^m	29

$$\frac{\partial n_m}{\partial t}+\frac{\partial \Gamma_m}{\partial x}=S_m \quad \ldots (3)$$

$$\frac{\partial \varepsilon_e n_e}{\partial t}+\frac{\partial \Gamma_{e\varepsilon}}{\partial x}=S_{e\varepsilon} \quad \ldots (4)$$

$$S_e = S_+ = n_e n_g K_{io} + n_e n_m K_{io}^m + n_m n_m K_{ci} \quad \ldots (5)$$

$$S_m = n_e n_g K_{ex} - n_e n_m K_{dex} - n_e n_m K_{io}^m - 2 n_m n_m K_{ci} - \frac{n_m}{\tau_m} \quad \ldots (6)$$

$$\Gamma_e = -n_e \mu_e E - \frac{\partial D_e n_e}{\partial x}, \quad \ldots (7)$$

$$\Gamma_+ = n_+ \mu_+ E - \frac{\partial D_+ n_+}{\partial x}, \quad \ldots (8)$$

$$\Gamma_m = -D_m \frac{\partial n_m}{\partial x} \quad \ldots (9)$$

$$\Gamma_{e\varepsilon} = -n_e \mu_{e\varepsilon} E - \frac{\partial D_{e\varepsilon} n_e}{\partial x}, \quad \ldots (10)$$

$$S_{e\varepsilon} = -e\Gamma_e E + \varepsilon_m n_e n_m K_{dex} + \varepsilon_{ci} n_m n_m K_{ci} - n_e P_{ec} - \varepsilon_m n_e n_g K_{ex} - \varepsilon_{io} n_e n_g K_{io} - (\varepsilon_{io} - \varepsilon_m) n_e n_m K_{io}^m \quad \ldots (11)$$

$$\frac{\partial^2 \varphi}{\partial x^2} = -\frac{e_o}{\varepsilon_o}(n_+ - n_e), \quad \ldots (12)$$

where (n_s), (Γ_s) and (S_s) are the particle densities, particle flux and source term with the subscript (s) electrons (e), positive ions (+) and metastable atoms (m). (n_g) denotes the neutral gas density. (ε_e) is the mean electron energy, ($\Gamma_{e\varepsilon}$) is the electron energy

flux, and the corresponding source term is ($S_{e\varepsilon}$). (φ) is the electrostatic potential, and (E) is the electric field strength. (μ_s) and (D_s), denote the mobility and diffusion coefficients of species (s). (ε_o) and (e_o) are the permittivity of free space and elementary charge, respectively.

($D_{e\varepsilon}$) and ($\mu_{e\varepsilon}$) represent the diffusion coefficient and mobility of the electron energy, respectively; and; ($D_{e\varepsilon} = D_e\varepsilon_e 5/3$); ($\mu_{e\varepsilon} = \mu_e\varepsilon_e 5/3$). and electron temperature is defined per $Te = 2\varepsilon_e / 3e_o$.

2.1 Boundary conditions

In this sub-section, we will present the initial and boundary conditions. There are a lot of boundary conditions and there are established in a different expressions. As ones given per Samir *et al.*[20] & Liu *et al.*[21]. Those boundary conditions are given hereafter:

The ion flux and electron temperature at each dielectric surfaces are given as follow:

$\Gamma_+ = n_+\mu_+E$ and $T_e = 0.5\,\text{eV}$

At dielectric surface (x=d): $\Gamma_e = -n_eK_s - \gamma\Gamma_+$

The discharge reactor is powered at (x=-Δ) by sinusoidal voltage $U(t) = U_a sin(2\pi ft)$ and at ground electrode (x=d+Δ) $U(t) = 0$.

The initial densities are chosen as Gaussian form; $n_e = n_+ = 10^7 + 10^9(1-x/d)^2(x/d)^2$ cm^{-3}[Ref.31-32].

Other boundary conditions cited per Hagelaar *et al.*[33]. Where the boundary conditions are given as follows:

The particle flux of electron and ion are written:

$$\Gamma_+.\nu = \frac{1-r_+}{1+r_+}\left(\left|n_+\mu_+E\right| + \frac{\upsilon_+^{th}n_+}{2}\right), \qquad \ldots (13)$$

$$\Gamma_e.\nu = \frac{1-r_e}{1+r_e}\left(\left|n_e\mu_eE\right| + \frac{\upsilon_e^{th}n_e}{2}\right) - \frac{2}{1+r_e}\gamma\max(\Gamma_+.\nu), \qquad \ldots (14)$$

where (ν) is equal to -1 at (x=0), and ($\nu = 1$) at x=d, and ($r_{e,+}$) is the reflection coefficient of electrons or ions and their values are given in Table 2.

The thermal velocity of electrons or ions is given by:

$$\upsilon_{e,+}^{th} = \sqrt{\frac{8k_bT_{e,+}}{\pi m_{e,+}}} \qquad \ldots (15)$$

Table 2 — Dielectric parameters and their references

Dielectric parameters		Value	Reference
Thickness		$\Delta = 1\text{mm}$	15
Reflection coefficient of electrons	Metallic	$r_e = 3\times10^{-1}$	34
	Dielectric	$r_e = 7\times10^{-1}$	34
Reflection coefficient of ions	Metallic	$r_+ = 5\times10^{-4}$	34
	Dielectric	$r_+ = 5\times10^{-3}$	34
Relative permittivity of dielectric	Borofloat glass	$\varepsilon_r = 4.6$	15
	Alumina	$\varepsilon_r = 10$	15
Reflection coefficient of metastable argon atoms		$r_m = 3\times10^{-1}$	19

The Gauss law [15] is applied in the presence of the dielectrics, to compute the accumulation of surface charges on the dielectrics as follow:

$$\varepsilon_r\varepsilon_oE_{diel}(x,t).\nu - \varepsilon_oE(x,t).\nu = \sigma_s(x,t)\ , \qquad \ldots (16)$$

where ($E_{diel}(x,t)$) is the electric field inside the dielectric and (ε_r) is their relative permittivity (see Table 2), and ($E(x,t)$) is the electric field related to the gas discharge. To compute the electric potential at the dielectrics (φ_0^t and φ_d^t), we have employed Eq. 16. The temporal evolution of the surface charge density ($\sigma_s(x,t)$) begins from particle currents breakthrough the dielectrics. This density is expressed by Becker *et al.*[19]

$$\frac{\partial\sigma_s(x,t)}{\partial t} = e_o\sum_j\Gamma_j(x,t).\nu \qquad \ldots (17)$$

The set of partial differential equations is discretized using the finite difference method. Moreover, the transport particle and energy equations have been discretized according to an exponential scheme[35-37]. The Poisson's equation has been discretized spatially by central difference technique. Both steps in time and within space grids are uniform and constants. The number of grid points in space is equal to 250 and per period time is equal to (4×10^3). The argon parameter transport are given in Table 3.

3. Results and discussion

Figure 2 shows the profiles of the electric potential as a function of the amplitude voltage at 3000th cycle CCRF argon dielectric barrier discharge. Those

Table 3 — Discharge configuration and argon physical characteristics applied in CCRF dielectric barrier discharge, E/n_g in Td

Symbol	Definition	Value	Refs.
D	Dielectric surfaces distance	1 (cm)	8-9
T_{gas}	Gas temperature	300 (K)	8-9
p	Pressure	1 (Torr)	8-9
U_a	Voltage amplitude	250, 350 and 450 (Volt)	8-9
f	Frequency	13.56 (MHz)	8-9
$n_g\mu_e$	Electron mobility	BOLSIG+	27-28
$n_g D_e$	Electron diffusivity	BOLSIG+	27-28
W_+	Ion drift velocity	$\frac{4E/n_g}{(1+(0.007E/n_g)^{1.5})^{0.33}}$	38
D_+	Ion diffusivity	$D_+ = \frac{\mu_+ T_{gas} k_b}{e_o}$	8-9
K_s	Electron recombination coefficient	1.19×10^{7} (cm s^{-1})	21
γ	Electron emission coefficient	0.06	8-9

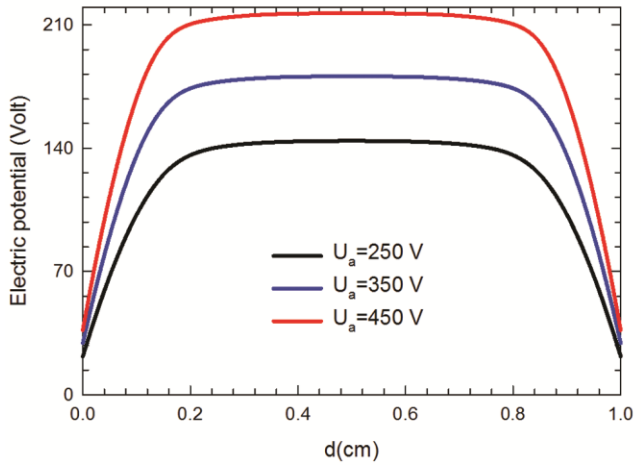

Fig. 2 — Electric potential profiles as a function of the amplitude voltage at 3000th cycle CCRF argon dielectric barrier discharge, and those profiles are provided in the cycle averaged diet.

profiles are given within the averaged cycle. We notice that the electrical potential is greater when the voltage amplitude is equal to 450 V than for the voltage amplitude of 350 V. And, the electric potential of the later is bigger than the one of the voltage amplitude of 250 V. When the voltage amplitude increases the chemical processes are amplified. Then, consequently the electric potential increases. Indeed, Fig. 2 illustrate this phenomenon: The electrical potential maximum values are 144.14, 180.76 and 216.57 V when the voltage amplitudes are

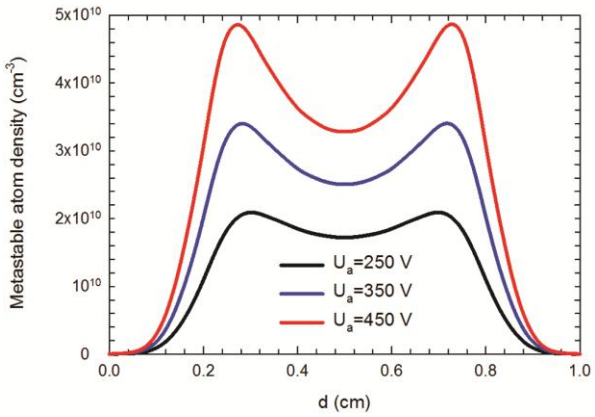

Fig. 3 — Metastable atom density curves at 3000th cycle CCRF argon dielectric barrier discharge as a function of the amplitude voltage. This picture provides the cycle averaged.

equal to 250, 350 and 450 V, respectively. The behavior of the electric potential is characterized by a bulk plasma region between two sheaths thicknesses where a maximum and minimum value of the potential are observed, respectively. Then, the landing potential is computed as a difference between the maximum and the minimum values of the electric potential. Thereby, the landing potential is equal to 122.46, 151.52 and 179.94 V when the voltage amplitude is equal to 250, 350 and 450 V, respectively. We notice that the landing potential increases with the increasing of the voltage amplitude.

Figure 3 represents the curve of the metastable atom density as a function of the amplitude voltage at 3000th cycle CCRF argon dielectric barrier discharge. This figure provides during a cycle-averaged. We remark that the metastable atom density has a symmetric form compared to the middle of the inter-electrode spacing. Consequently, the metastable atoms density is characterised by two maximum values. We can see that the metastable atoms density increases with increasing amplitude voltage. This is due to the increased excitation process. The maximum of the metastable atoms density evolves from (2.09×10^{10}) to (4.86×10^{10}) (cm^{-3}) when the amplitude voltage evolves from 250 to 450 V.

Figure 4 confers on the outlines of the electron temperature as a function of the amplitude voltage at 3000th cycle CCRF argon dielectric barrier discharge, and these profiles are computed on a cycle-averaged regime. As one can see, the electron temperature profile is characterized by two peaks between them decreasing temperature. This distribution is caused by a higher gradient of potential at both electrodes and

then a strong electron flux. Thereby, a heating phenomenon occurred at both electrodes. In contrary, the cooling phenomenon created by the electron density and the argon ground state, as well as threshold ionisation or excitation which are weakling in the sheath thickness. In the bulk plasma region the cooling phenomenon is greater due to the presence of a higher electron density. We remark that the electron temperature increase with the increasing of the amplitude voltage. Moreover, this augmentation is concentrated only in the sheath thickness. The electron temperature is independent of the amplitude voltage in the bulk plasma region. As results, the heating phenomenon is that the most dominant in the behaviour argon DBD's discharge.

In Fig. 4, the maximum of the electron temperature increases from 9.16 to 19.72 eV when the amplitude voltage changes from 250 to 450 V.

Table 4 illustrate the discharge behaviour, where the plasma density and the electric field are given as a function of the amplitude voltage at 3000 cycle averaged in CCRF argon dielectric barrier discharge. As one can see the plasma density increase with amplitude voltage from (6.61×10^{9}) to (1.39×10^{10}) (cm^{-3}). This behaviour can be explained by an increase of chemical processes due to the augmentation of the amplitude voltage. Where collisions processes (ionisation, stepwise ionisation and the chemo ionisation) occurring then, inducing-to raise the particle densities. As consequence, the electric field increase with amplitude voltage from 997.08 to 1685.10 V/cm.

Table 4 — Summary of the plasma density and the electric field as a function of the amplitude voltage at 3000 cycle averaged in CCRF argon dielectric barrier discharge

Amplitude voltage (V)	Plasma density (cm^{-3})	Electric field (V/cm)
250	6.61×10^{9}	997.08
350	1.02×10^{10}	1344.80
450	1.39×10^{10}	1685.10

In order to valid our numeric code, we have investigated the discharge without dielectric and have compared our results to those given by Park & Economou[39], Meyyappan & Govindan[40], Hwang *et al.*[41], Surendra & Vender[42], and Surendra *et al.*[43]. The results are coherent.

Figure 5 represents the effect of the amplitude voltage on the applied and gap voltages as a function of reduced periodic of CCRF argon dielectric barrier discharge at 3000th cycles. As one can see the applied voltage (U(t)) for different amplitude has still same observed behaviour at each period. This is noticeable due to the expression form of the (U(t)). The gap voltage ($U_g(t)$) is as follow: ($U_g(t)=\varphi_0^t-\varphi_d^t$). Consequently, gap voltage is less than applied voltage. In one hand, we notice that the resulting form of the gap voltage is sinusoidal because the source voltage has sinusoidal form. Consequently, the amplitude of gap voltage is reached to 224.42, 311.69 and 398.76 V when the amplitude voltage equal to 250, 350 and 450 V, respectively.

As a result, the difference voltage between them is about of 25.58, 38.30 and 51.23 V. We remark that the difference voltage increase with the increasing of the amplitude voltage.

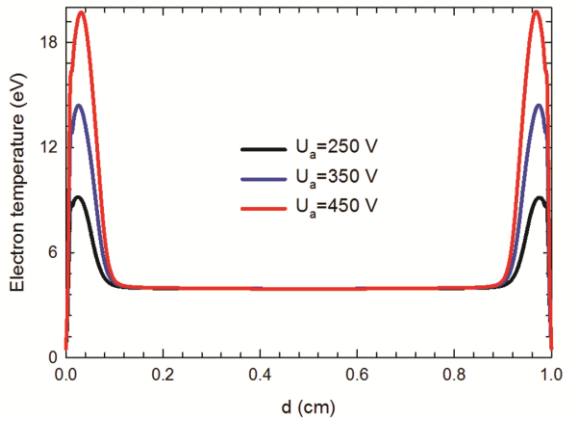

Fig. 4 — Electron temperature profiles as a function of the voltage amplitude at 3000th cycle CCRF argon dielectric barrier discharge. These profiles are computed in the cycle-averaged regime.

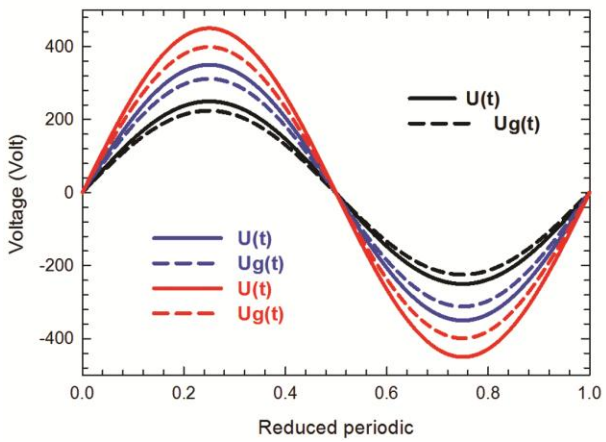

Fig. 5 — Effect of the amplitude voltage on the applied and gap voltages as a function of reduced periodic of CCRF argon dielectric barrier discharge at 3000th cycles.

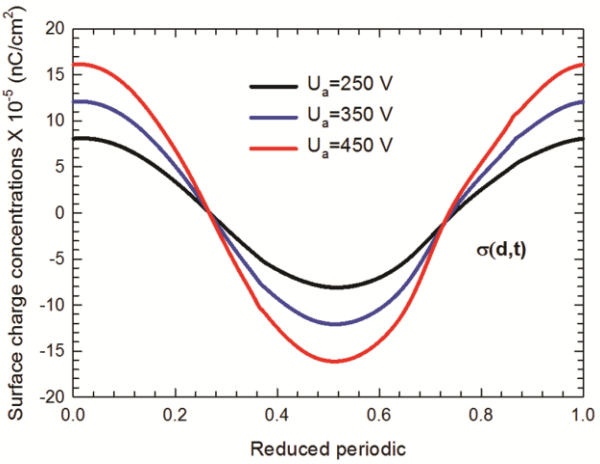

Fig. 6 — Effect of the amplitude voltage on the surface charge concentrations $\sigma_s(d,t)$ as a function of reduced periodic of CCRF argon dielectric barrier discharge at 3000th cycles.

Figure 6 shows the effect of the amplitude voltage on the surface charge concentrations ($\sigma_s(d,t)$) as a function of reduced periodic of CCRF argon dielectric barrier discharge at 3000th cycles. The morphology of the surface charge concentrations ($\sigma_s(d,t)$) strictly follows the gap voltage structure. The surface concentrations reflect the precipitation of the charged particle on the dielectrics. Furthermore, this precipitation increases in the time. As one can see the surface charge concentration ($\sigma_s(d,t)$) increases with the increasing amplitude voltage. Where the maximum increases from 8.11 $\times 10^{-5}$ to 16.14 $\times 10^{-5}$ (nC/cm^2) when the amplitude voltage change from 250 to 450 V. This is due to the augmentation of the electric field at the electrodes.

Figure 7 shows the effect of the amplitude voltage on the surface charge concentrations ($\sigma_s(o,t)$) as a function of reduced periodic of CCRF argon dielectric barrier discharge at 3000th cycles. As one can see the morphology of the surface charge concentrations ($\sigma_s(o,t)$) has the same behaviour as ($\sigma_s(d,t)$), with reversed polarity, *i.e.*, while the surface charge concentration ($\sigma_s(d,t)$) is at maximum value, ($\sigma_s(o,t)$) is at minimum value, and vice versa. The effect of the amplitude voltage on the surface charge concentration ($\sigma_s(o,t)$) is similar to the effect on ($\sigma_s(d,t)$). The amplitude of ($\sigma_s(o,t)$) evolves from 8.10$\times 10^{-5}$ to 16.11$\times 10^{-5}$ (nC/cm^2) when the amplitude voltage changes from 250 to 450 V. The observed increase on the amplitude of $\sigma_s(o,t)$ is due

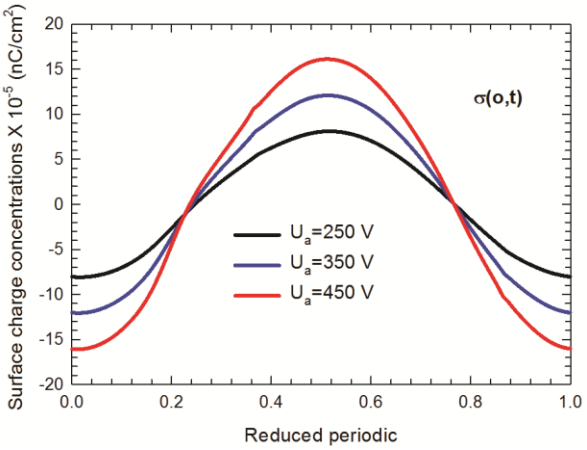

Fig. 7 — Effect of the amplitude voltage on the surface charge concentrations $\sigma_s(o,t)$ as a function of reduced periodic of CCRF argon dielectric barrier discharge at 3000th cycles.

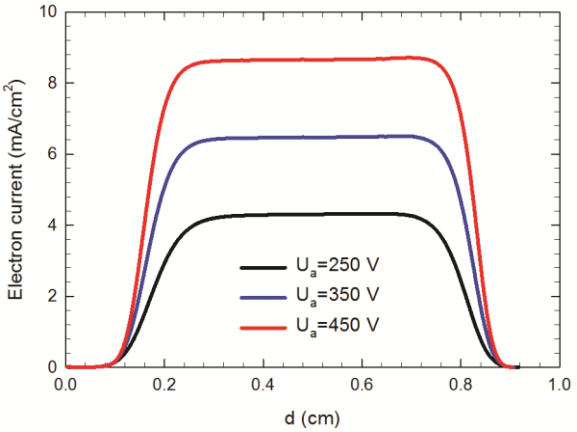

Fig. 8 — Effect of the amplitude voltage on electron current at 3000th cycle CCRF argon dielectric barrier discharge at the phase $wt = \pi$.

to the augmentation of the electric field at the electrodes.

Fig. 8 illustrates the effect of the amplitude voltage on electron current at 3000th cycle CCRF argon dielectric barrier discharge at the phase ($wt = \pi$). We remark that the electron current is characterized by two-sheath thickness located at both electrodes, and plasma region. As one can see that the effect of the amplitude voltage is independent of both sheath thickness, but in the plasma region the electron current increase with the increasing of the amplitude voltage because of the augmentation of the electron density that is present. Moreover, we notice that the electron current is quasi constant in the plasma region.

One can notice, that the maximum of the electron current is 4.31, 6.47 and 8.65 (mA/cm^2) for the amplitude voltage 250, 350 and 450 V, respectively.

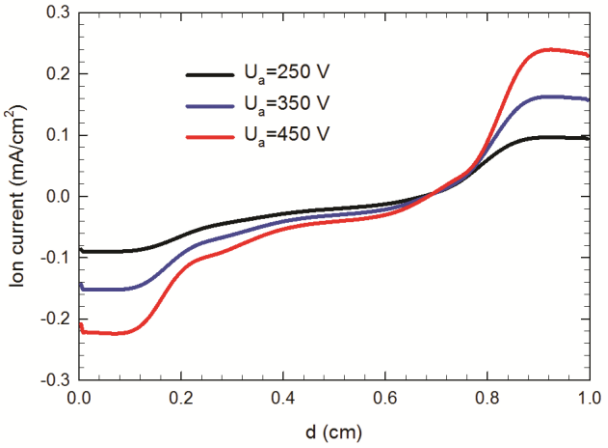

Fig. 9 — Effect of the amplitude voltage on the ion current at 3000th cycle CCRF argon dielectric barrier discharge at the phase $wt = \pi$.

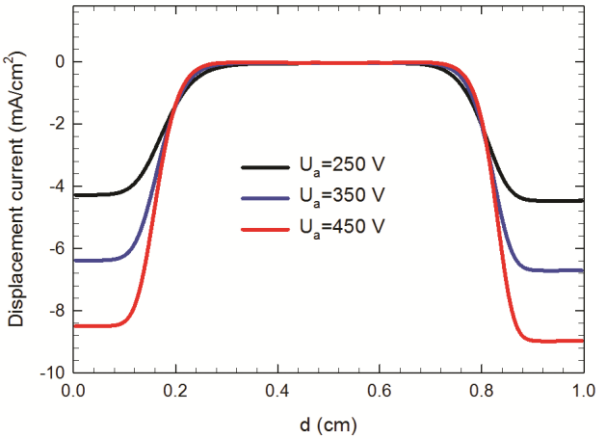

Fig. 10 — Effect of the amplitude voltage on displacement current at 3000th cycle CCRF argon dielectric barrier discharge at the phase $wt = \pi$.

Figure 9 shows the effect of the amplitude voltage on the ion current at 3000th cycle CCRF argon dielectric barrier discharge at the phase ($wt = \pi$). We notice that the spatial distribution of the ion current is symmetric at the middle of the inter-electrode spacing. This is due to the electric field behaviour on the ion current. As one can see the ion current increases when the amplitude voltage increases due to the augmentation of the ion density and the electric field. The maximum of the ion current increases from 0.09 to 0.24 (mA/cm^2) when the amplitude voltage changes from 250 to 450 V.

Figure 10 shows the effect of the amplitude voltage on displacement current at 3000th cycle CCRF argon dielectric barrier discharge at the phase ($wt = \pi$). We remark that the spatial distribution of the displacement current is characterized by two-sheath thickness located at both electrodes, between them a plasma region. However, as one can observe the behaviour of the displacement current is different to that of the electron current. On the one hand, the effect of the amplitude voltage on the displacement current in the plasma region is independent, *i.e.*, regardless of the amplitude voltage the displacement current does not change. On the other hand, the displacement current increase with the increasing of the amplitude voltage. It is obvious that the maximum of the displacement current is 4.28, 6.38 and 8.50 (mA/cm^2) for the effect of the amplitude voltage 250, 350 and 450 V, respectively. In the plasma area the displacement current is null regardless of the amplitude voltage.

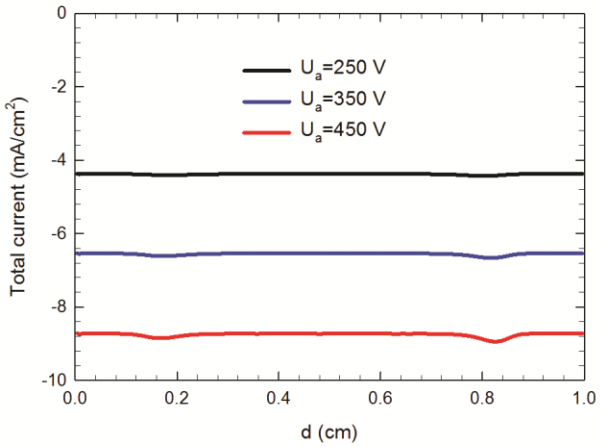

Fig. 11 — Effect of the amplitude voltage on total current at 3000th cycle CCRF argon dielectric barrier discharge at the phase $wt = \pi$.

Figure 11 shows the effect of the amplitude voltage on total current at 3000th cycle CCRF argon dielectric barrier discharge at the phase ($wt = \pi$). The total current represents the sum of the electron, ion and metastable atom as well as displacement currents. Furthermore, the metastable atom current is negligible, and it is not show. Therefore, the current fall of both electron and displacement currents is faded away between them and the total current is constant in inter-electrodes spacing. It is obvious that the total current at the phase ($wt = \pi$) is -4.37, -6.54 and -8.73 (mA/cm^2) for the amplitude voltage 250, 350 and 450 V, respectively.

4 Conclusions

Although, three moments of Boltzmann's equation with Poisson's equation describe capacitively coupled

argon glow discharge driven by radio frequency power at low pressure with dielectrics. In addition, the metastable atom density is introduced again in the model. Mainly to describe the model, we have used the particle flux expression explaining the electrons and ions kinetic in both electrodes. Furthermore, the Gauss law explain the accumulation of the charged particle on the dielectrics. The effect of boundary conditions in the presence of dielectric is well defined from the spatial distribution of the surface charge concentrations and the gap voltage in time. The effect of the amplitude voltage on the discharge behaviour is presented within the cycle-averaged. As a result, the metastable atom density, electron temperature and electric potential increases when the amplitude voltage increases. From there the surface charge concentration and the gap voltage increase again.

References

1 Samir T, Liu Y, Zhao L L & Zhou Y W, *Chin Phys B*, 26 (2017) 115201.
2 Donko Z, *Phys Rev E*, 57 (1998) 7126.
3 Bouchikhi A, *Indian J Pure Appl Phys*, 60 (2022) 163.
4 Zhao L L, Liu Y & Samir T, *Chin Phys B*, 26 (2017) 125201.
5 Meyyappan M & Kreskovsky J P L, *J Appl Phys*, 68 (1990) 1506.
6 Hechelef B & Bouchikhi A, *Acta Physica Polonica A*, 136 (2019) 855.
7 Becker M M & Loffhagen D, *AIP Advances*, 3 (2013) 012108.
8 Alili T, Bouchikhi A & Rizouga M, *Can J Phys*, 94 (2016) 731.
9 Becker M M, Loffhagen D & Schmidt W, *Comput Phys Commun*, 180 (2009) 1230.
10 Hechelef B & Bouchikhi A, *Plasma Sci Technol*, 20 (2018) 115401.
11 Bouchikhi A, *Can J Phys*, 96, (2018) 62.
12 Bouchikhi A, *IEEE Trans Plasma Science*, 9 (2019) 4260.
13 Bouchikhi A, *Plasma Sci Technol*, 19 (2017) 095403.
14 Lin Y & Adomaitis R A, *J Comp Phys*, 171 (2001) 731.
15 Loffhagen D, Becker M M, Czerny A K, Philipp J & Klages C, *Contrib Plasma Phys*, 58 (2018) 337.
16 Ponduri S, Becker M M, Welzel S, van de Sanden M C M, Loffhagen D & Engeln R, *J Appl Phys*, 119 (2016) 093301.
17 H€oft H, Kettlitz M, Becker M M, Hoder T, Loffhagen D, Brandenburg R & Weltmann K D, *J Phys D Appl Phys*, 47 (2014) 465206.
18 Eslami E, Barjasteh A & Morshedian N, *Plasma Phys Rep*, 41 (2015) 519.
19 Becker M M, Hoder T, Brandenburg R & Loffhagen D, *J Phys D Appl Phys*, 46 (2013) 355203.
20 Samir T, Liu Y & Zhao L L, *IEEE Trans Plasma Science*, 46 (2018) 1738.
21 Liu Q, Liu Y, Samir T & Ma Z, *Phys Plasmas*, 21 (2014) 083511.
22 Becker M M, Kählert H, Sun A, Bonitz M & Loffhagen D, *Plasma Sources Sci Technol*, 26 (2017) 044001.
23 Barjasteh A & Eslami E, *Plasma Chem Plasma Process*, 38 (2018) 261.
24 Barjasteh A, Eslami E & Morshedian N, *Phys Plasmas*, 22 (2015) 073508.
25 Kolokolov N B, Kudrjavtsev A A & Blagoev A B, *Phys Scri*, 50 (1994) 371.
26 Rafatov I, Bogdanov E A & Kudryavtsev A A, *Phys of Plasma*, 19 (2012) 093503.
27 Hagelaar G J M & Pitchford L C, *Plasma Sources Sci Technol*, 14 (2005) 722.
28 http://nl.lxcat.net/home/
29 Vriens L & Smeets A H M, *Phys Rev A*, 22 (1980) 940.
30 Van G W & Bogaerts A, *J Phys D Appl Phys*, 47 (2014) 079502.
31 Bouchikhi A & Hamid A, *Plasma Sci Technol*, 12 (2010) 59.
32 Bouchikhi A, *Plasma Sci. Technol*, 14 (2012) 965.
33 Hagelaar G J M, Kroesen G M W, van Slooten U & Schreuders H, *J Appl Phys*, 88 (2000) 2252.
34 Golant V E, Zilinskij A P, Sacharov I E & Brown S C, Fundamentals of Plasma Physics, New York: Wiley, (1980).
35 Scharfetter D L & Gummel H K, *IEEE Trans Elec Dev*, 16 (1969) 64.
36 Bouchikhi A, *Indian J Phys*, 94 (2020) 353.
37 Bouchikhi A, *Indian J Phys*, 96 (2022) 1443.
38 Phelps A & Petrovic´ Z, *Plasma Sources Sci Technol*, 8 (1999) R21.
39 Park S K & Economou D J, *J Appl Phys*, 68 (1990) 4888.
40 Meyyappan M & Govindan T R, *J Appl Phys*, 74 (1993) 2250.
41 Hwang S W, Lee H J & Lee H J, *Plasma Sources Sci Technol*, 23 (2014) 065040.
42 Surendra M & Vender D, *Appl Phys Lett*, 65 (1994) 153.
43 Surendra M, Graves D & Plano L, *J Appl Phys*, 71 (1992) 5189.